analytical chemistry

Article

pubs.acs.org/ac

Biomimetic Superoxide Dismutase Stabilized by Photopolymerization for Superoxide Anions Biosensing and Cell Monitoring

Ling Yuan, Suli Liu, Wenwen Tu, Zengsong Zhang, Jianchun Bao, and Zhihui Dai*

Jiangsu Key Laboratory of Biofunctional Materials, School of Chemistry and Materials Science, Nanjing Normal University, Nanjing 210023, P. R. China

Supporting Information

ABSTRACT: Photopolymerization strategy, as one of the immobilization methods, has attracted considerable interest because of some advantages, such as easy operation, harmlessness to the biomolecules, and long storage stability. (*E*)-4-(4-Formylstyryl) pyridine (formylstyrylpyridine) was prepared through Heck reaction and used as a photopolymer material to immobilize biomimetic superoxide dismutase under ultraviolet irradiation (UV) irradiation in a short time. The styrylpyridinium moiety of Formylstyrylpyridine was photoreactive and formed a dimer under UV irradiation. $Mn_2P_2O_7$ multilayer sheet, a novel superoxide dismutase mimic, was synthesized. The formed photopolymer can immobilize $Mn_2P_2O_7$ firmly under UV irradiation. On the basis of high catalytic activity of $Mn_2P_2O_7$ biomimetic enzyme and long-term stability of $Mn_2P_2O_7$−formylstyrylpyridine film, after introducing multiwalled carbon nanotubes (MWCNTs), a novel electrochemical biosensing platform called MWCNTs/$Mn_2P_2O_7$−formylstyrylpyridine for superoxide anion ($O_2^{\bullet-}$) detection was constructed. The biosensor displayed good performance for $O_2^{\bullet-}$ detection and provided a reliable platform to adhere living cells directly on the modified electrode surface. Therefore, the biosensor was successfully applied to vitro determination of $O_2^{\bullet-}$ released from living cells, which had a promising prospect for living cells monitoring and diagnosis of reactive oxygen species-related diseases.

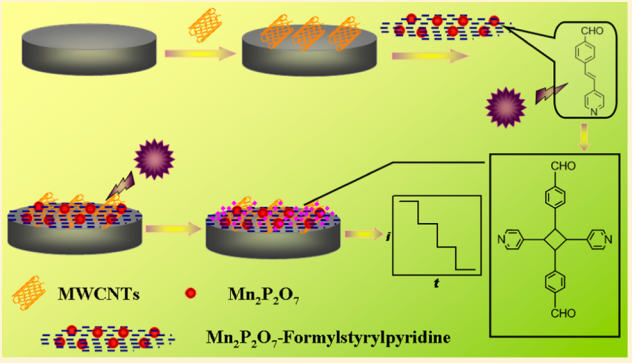

Immobilization methods have been considered as an essential factor to develop efficient biosensors with excellent properties, such as good operational stability, short response time, high sensitivity and selectivity, and good reproducibility and storage stability.[1] Various immobilization strategies, such as adsorption,[2,3] covalent coupling,[4−6] entrapment,[7−9] cross-linking,[10,11] and affinity,[12,13] have been developed to construct biosensors. Adsorption technique presented drawbacks, such as desorption of the immobilized biomolecules, nonspecific adsorption of other substances, and poor operational and storage stability. Covalent coupling method might couple with toxic products and some groups need to be activated in the process. Cross-linking strategy might distort the conformation and active sites of the active enzymes. Affinity method limited the kind of the immobilized biomolecules because corresponding biomolecules were oriented and site-specific.[1,2,14,15] Entrapment methods including electropolymerization, photopolymerization, sol−gel process and entrapment in a carbon paste have attracted increasing attention due to some advantages compared with other immobilization methods mentioned above. First, this immobilization method was easy and simple to handle. Conductive materials, enzymes and signaling molecules could be added in the same sensing layer simultaneously. Second, the enzymatic activity was preserved, because there was no modification of the enzyme during the immobilization process. Third, biosensors showed good operational and storage stability due to enzymes physically entrapped.[1,15] Besides these three outstanding features, photopolymerization method could make the monomer form polymer film under ultraviolet (UV) irradiation in a short time and the film presented a higher mechanical stability than those of some hydrogels that were used for enzyme immobilization.[1] The styrylpyridinium (SbQ) moiety of the monomer was photoreactive and could form a dimer under UV irradiation.[16] According to this principle, a novel material called (*E*)-4-(4-formylstyryl) pyridine (Formylstyrylpyridine), which contained SbQ moiety, was introduced to prepare polymer film under UV irradiation in this work.

Superoxide anion ($O_2^{\bullet-}$) is one of the most active reactive oxygen species (ROS) in biological systems.[17,18] Excess $O_2^{\bullet-}$ may bring oxidative damage to lipids, nucleic acids, and proteins, resulting in mutagenesis, cell death, and some diseases.[19,20] Therefore, a variety of techniques including electron spin resonance trapping,[21,22] chromatograph,[23,24]

Received: December 3, 2013
Accepted: April 28, 2014
Published: April 28, 2014

   dx.doi.org/10.1021/ac403920q | *Anal. Chem.* 2014, 86, 4783−4790

spectrophotometry,[25] fluorescence,[26−28] and chemiluminescence[29] have been developed for reliable detection of $O_2^{\bullet-}$. In addition to these techniques, electrochemical methods have received extensive attention owing to their intrinsic advantages including direct and real-time detection, high sensitivity, facile operation and so on.[30−36] Recently, the electrochemical measurements of $O_2^{\bullet-}$ based on the incorporation of enzymes, such as superoxide dismutase (SOD) onto electrodes have been paid more attention due to its good selectivity and high sensitivity.[37,38] However, the preparation and purification of enzymes are usually expensive and time-consuming.[39−41] Meanwhile, enzymes are of easy denaturation and leakage during their immobilization and storage procedure.[42,43] Therefore, a large amount of SOD mimics have been developed because of their natural stable property, high catalytic activity, long-term stability and low cost.[44] Among the SOD mimics, MnSOD mimics have attracted increasing attention, owing to their lower toxicity in comparison to copper or iron mimics.[45,46] Recently, a lot of MnSOD mimics, for example, manganous phosphate and manganese(II) complexes of scorpiand-like azamacrocycles, have been synthesized and applied to monitor $O_2^{\bullet-}$.[30,47] However, Mn^{2+} needed to be confined in the Nafion-modified TiO_2 nanoneedles when manganous phosphate was formed and ligands needed to be synthesized when manganese(II) complexes of scorpiand-like azamacrocycles was synthesized. To simplify the complex synthesis process, manganous pyrophosphate ($Mn_2P_2O_7$) used as MnSOD mimic in phosphate solution was expected.

In this work, SOD mimic was stabilized by a photopolymer material, Formylstyrylpyridine, which was generated from ultraviolet (UV) irradiation. After introducing multiwalled carbon nanotubes (MWCNTs), a novel electrochemical biosensor was developed to detect $O_2^{\bullet-}$ (Scheme 1). As expected, the $Mn_2P_2O_7$−formylstyrylpyridine film exhibited long-term stability, durability and good biocompatibility. MWCNTs had large surface area and good electronic conductivity which could enhance the electrochemical response. MWCNTs/$Mn_2P_2O_7$−formylstyrylpyridine films provided a reliable platform to adhere living cells directly on the modified electrode surface for real-time monitoring of $O_2^{\bullet-}$. On the other hand, this $O_2^{\bullet-}$ biosensor exhibited remarkable analytical performance, including good selectivity, wide linear range, low detection limit and so on. Thus, a reliable and durable approach for real-time and in situ detection of $O_2^{\bullet-}$ in cells was designed in this work.

Scheme 1. Schematic diagram for the construction of the biosensor

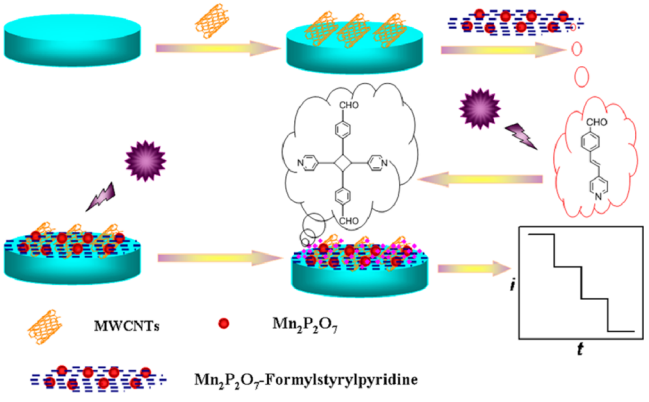

EXPERIMENTAL SECTION

Reagents and Materials. Potassium hyperoxide (KO_2), dopamine (DA), ascorbic acid (AA), L-cysteine (Cys), peroxynitrite ($ONOO^-$), ferricytochrome *c*, and phorbol 12-myristate 13-acetate (PMA) were obtained from Sigma and used without further purification. MWCNTs (φ = 10−20 nm) were obtained from Nanotech Port Co., Ltd. (Shenzhen, China). $Mn(CH_3COO)_2$ was obtained from Alfa Aesar. Dimethyl sulfoxide (DMSO), polyphosphoric acid ($H_6P_4O_{13}$), K_3PO_4, and H_2O_2 were purchased from Sinopharm Chemical Reagent Co., Ltd. A stock solution of KO_2 was prepared by adding KO_2 to DMSO (N_2-saturated and stored together with molecular sieve 4 Å), and then sonicating for 2 min. $OH^{\bullet}$ was generated in H_2O_2 (10 mmol L^{-1}) catalyzed by Fe^{2+}. 3-(4,5-Dimethylthiazol-2-yl)-2,5-diphenyltetrazolium bromide (MTT) cell proliferation and cytotoxicity assay kit was purchased from Nanjing KeyGEN Biotech. Co., Ltd. (Nanjing, China). All other chemicals were of analytical grade. Aqueous solution was prepared with doubly distilled water (DDW) and pH of K_3PO_4 solution was adjusted by pH meter.

Preparation of Formylstyrylpyridine. The recipe of the preparation of Formylstyrylpyridine was developed by our lab. A sealed tube (25 mL) initially filled with 4-bromobenzaldehyde (92.5 mg, 0.5 mmol), 4-vinylpyridine (52.57 mg, 0.5 mmol), $Pd(OAc)_2$ (1.344 mg, 0.006 mmol, 1.2 mol %), and triphenylphosphine (3.144 g, 0.012 mmol, 1.2 mol %) was evacuated and purged with nitrogen gas three times. Triethylamine (0.34 mL, 2.5 mmol) and tetrahydrofuran (2 mL) were added to the system. The reaction mixture was stirred at 60 °C for 15 h and then was extracted with dichloromethane, being washed and dried for later use. The filtrate was concentrated by vacuum and separated on a silica gel column using hexane/ethyl acetate as eluent to give the corresponding pure product (yellow solid, 62.7 mg, 60% yield).

Preparation of $Mn_2P_2O_7$ Sheets. The recipe of the preparation of $Mn_2P_2O_7$ was developed also by our lab. In a typical synthesis, Pluronic P123 (20 mL, 0.0104 mol L^{-1}, $EO_{20}PO_{70}EO_{20}$, Aldrich, M_{av} =5800 g mol^{-1}) ethanol solution and $H_6P_4O_{13}$ (2.6 mL) were mixed under stirring for 0.5 h at room temperature. Then $Mn(CH_3COO)_2$ (1.20 g) was added to the above solution and stirred for 1 h at room temperature. The pink resulting transparent solution was transferred to a 50 mL Teflon-lined autoclave. The autoclave was sealed and maintained at 100 °C for 12 h, and then it was allowed to cool to room temperature. After the deposits were collected and washed with absolute ethanol for several times to remove surfactants, the deposits were centrifuged and dried at 40 °C to obtain $Mn_2P_2O_7$. This as-synthesized material of $Mn_2P_2O_7$ was gray powder.

Preparation of Formylstyrylpyridine and $Mn_2P_2O_7$−Formylstyrylpyridine Film. Formylstyrylpyridine was solved in ethanol solution to obtain 0.5 mmol L^{-1} formylstyrylpyridine ethanol solution. Five milligrams of $Mn_2P_2O_7$ was mixed with 2 mL of formylstyrylpyridine ethanol solution and ultrasonicated to obtain a uniform $Mn_2P_2O_7$−formylstyrylpyridine suspension. Then 10 μL of formylstyrylpyridine ethanol solution was dropped on a quartz substrate without or with UV irradiation for 12 min to obtain formylstyrylpyridine film. $Mn_2P_2O_7$−Formylstyrylpyridine film was prepared by dropping 10 μL of $Mn_2P_2O_7$−formylstyrylpyridine suspension on a quartz substrate without or with UV irradiation for 12 min.

dx.doi.org/10.1021/ac403920q | Anal. Chem. 2014, 86, 4783−4790

Preparation of MWCNTs Suspension. The MWCNTs suspension was prepared according to the previous report[48] with a little modification. First, MWCNTs (15 mg) were purified through reflux in concentrated HNO_3–H_2SO_4 (30 mL, *V*/*V*, 1:1) mixture for 12 h at 55 °C. Then the reaction mixture was dried after washing with DDW until pH 7.0. Finally, the purified MWCNTs (1 mg) were added into DDW (2 mL) and ultrasonicated to obtain a uniform and black MWCNTs suspension.

Preparation of the Modified Electrodes. The GCE was polished with 1.0, 0.3, and 0.05 μm α–Al_2O_3 powder, respectively. After sonication in water, the electrode was rinsed with DDW and allowed to dry under a stream of nitrogen gas. MWCNTs suspension (5 μL) was dropped on the pretreated GCE and dried in a desiccator to obtain MWCNTs modified electrode. $Mn_2P_2O_7$ (5 mg) was mixed with Formylstyrylpyridine ethanol solution (2 mL, 0.5 mmol L^{-1}) and ultrasonicated to obtain a uniform $Mn_2P_2O_7$–formylstyrylpyridine suspension. Then $Mn_2P_2O_7$–formylstyrylpyridine suspension (5 μL) was dropped on MWCNTs to obtain MWCNTs/$Mn_2P_2O_7$–formylstyrylpyridine modified electrode. Finally, MWCNTs/$Mn_2P_2O_7$–Formylstyrylpyridine was under UV irradiation performed with a high-pressure mercury lamp (365 nm) for 12 min to obtain MWCNTs/$Mn_2P_2O_7$–formylstyrylpyridine modified electrode.

Apparatus and Measurements. Electrochemical measurements including cyclic voltammetry (CV) and amperometric *i*–*t* curve were performed on a CHI 660D electrochemical workstation (CH Instruments Inc., USA). The CV experimental parameters were as follows. Scan rate was 100 mV s^{-1} and potential scanning range was 0.1–0.9 V. The applied potential of amperometric i-t curve was 0.15 V. The supporting electrolyte of CV and *i*–*t* experiments was K_3PO_4 solution (pH 7.4). Electrochemical impedance spectroscopy (EIS) was performed on an Autolab potentiostat/galvanostat PGSTAT302N (Eco chemie, BV, The Netherlands). A three electrode electrochemical system was composed of a saturated calomel electrode (SCE) as the reference electrode, a platinum wire as the auxiliary electrode, and a bare or modified GCE (*d* = 3 mm) as the working electrode. The EIS experiments were carried out under open circuit conditions, the voltage frequencies ranged from 0.1 to 10^5 Hz and the AC voltage amplitude was 5 mV. The supporting electrolyte was $K_3[Fe(CN)_6]$ and $K_4[Fe(CN)_6]$ (5 mmol L^{-1}, 1:1) solution containing KCl (0.1 mol L^{-1}). Ultraviolet–visible (UV–vis) absorption spectra were recorded using a Cary 5000 UV–visible/near-infrared spectrophotometer (Varian, USA). UV irradiation for the dried $Mn_2P_2O_7$–Formylstyrylpyridine film was performed with a high-pressure mercury lamp (365 nm, 12 min) and the absorbance was recorded at wavelength from 200 to 600 nm. The transmission electron microscopy (TEM) image was examined by a JEM-200CX instrument (Japan), using an accelerating voltage of 80 kV. The scanning electron microscopy (SEM) images of the formed complex film were recorded on a JSM-7600F field emission scanning electron microscopy (JEOL, Japan) at an accelerating voltage of 10 kV. ^{1}H nuclear magnetic resonance (^{1}HNMR) (400 MHz, $CDCl_3$) was recorded at an AVANCE 400 nuclear magnetic resonance spectrometer (Bruker, Switzerland). The X-ray diffraction (XRD) patterns were characterized by a powder sample in 2θ ranging from 10 to 90°, using a D/max 2500VL/PC diffractometer (Japan) equipped with graphite monochromatized Cu Kα radiation (λ = 1.54060 Å).

Preparation of $O_2^{\bullet-}$ Solutions and Different Concentrations of Interfering Species. The $O_2^{\bullet-}$ solutions were prepared by adding KO_2 stock solution, which was N_2-saturated. The concentration of $O_2^{\bullet-}$ was monitored by recording the reduction of ferricytochrome *c* spectrophotometrically at 550 nm. The extinction coefficient of ferricytochrome *c* is 21.1 mM^{-1} cm^{-1}. All measurements were carried out at room temperature. The experimental solutions were deaerated by bubbling highly pure nitrogen for 20 min, and a nitrogen atmosphere was kept over the solution during the measurements. A stock solution of 5 mmol L^{-1} DA, 10 mmol L^{-1} AA, 5 mmol L^{-1} Cys, 10 mmol L^{-1} H_2O_2, and 10 mmol L^{-1} Fe^{3+} was prepared by adding corresponding DA, AA, Cys, H_2O_2, and $FeCl_3$ to DDW, respectively. A stock solution of $OH^{\bullet}$ was generated in 10 mmol L^{-1} H_2O_2 catalyzed by Fe^{2+}. A stock solution of 10 mmol L^{-1} $ONOO^-$ was generated by diluting commercially available peroxynitrite solution with 0.1 mol L^{-1} NaOH solution. The interfering species including 5 μmol L^{-1} DA, 10 μmol L^{-1} AA, 5 μmol L^{-1} Cys, 10 μmol L^{-1} H_2O_2, 10 μmol L^{-1} $OH^{\bullet}$, 10 μmol L^{-1} $ONOO^-$, and 10 μmol L^{-1} Fe^{3+} was prepared by adding 2 μL of the corresponding stock solution to 2 mL of 50 mmol L^{-1} K_3PO_4 solution (pH 7.4). O_2 was added by bubbling highly pure oxygen for 20 min, and an oxygen atmosphere was kept over the solution during the measurement. At room temperature and pressure, the saturated concentration of O_2 was about 8.25 mg L^{-1} (258 μmol L^{-1}).

Culture of Cells. The HeLa cells were purchased from Shanghai Institute of cell library. The cells were cultured in DMEM supplemented with 10% fetal bovine serum (FBS), penicillin (100 U mL^{-1}), and streptomycin (100 U mL^{-1}) at 37°C in a humidified atmosphere containing CO_2 (5%). Glutaraldehyde could enhance the stability of cells and decrease the gap between the cells and the modified electrodes.[49,50] Adhered cells (5 mL) were fixed with 0.5 μL of glutaraldehyde (2%) for 20 min at room temperature. The final concentration of glutaraldehyde was 0.0002%. After that the pretreated cells (0.5 mL, 1 × 10^5 cells mL^{-1}) were plated on the modified electrode for electrochemical determination of $O_2^{\bullet-}$. Four microliters of 100 μg mL^{-1} PMA was added to 1 mL of K_3PO_4 solution (50 mmol L^{-1}) containing 50 mmol L^{-1} glucose. Real sample measurements were performed in K_3PO_4 (50 mmol L^{-1}) containing glucose (50 mmol L^{-1}).

MTT Assay. The cytotoxicity of glutaraldehyde was analyzed by using MTT.[51,52] For the MTT assay, HeLa cells were seeded in 96-well plates (1 × 10^4 cells per well). The cells were treated with various concentrations of glutaraldehyde (0, 1%, 0.2%, 0.02%, 0.002%, 0.0002% and 0.00002%) for 30 min. After that, MTT (0.2 mg/mL) was added to each well and incubated for 4 h. The supernatant was removed and the formazan crystals were dissolved in DMSO. Cell viability was assessed by measuring the absorbance at 550 nm using a microplate reader.

RESULTS AND DISCUSSION

Characterization. Formylstyrylpyridine was characterized by nuclear magnetic resonance spectrometer. ^{1}HNMR (400 MHz, $CDCl_3$): δ = 10.01 (s, 1H), 8.64 (d, *J* = 4.4 Hz, 1H), 7.89 (d, *J* = 8.0 Hz, 2H), 7.68–7.73 (m, 4H), 7.42 (d, *J* = 8.00 Hz, 1H), 7.30 (d, *J* = 16.0 Hz, 1H), 7.21 (t, *J* = 6.8 Hz, 1H) ppm.

Figure 1A showed the spectral change on UV–vis absorption of the Formylstyrylpyridine film on a quartz substrate before (curve a) and after (curve b) UV irradiation. The decrease of the absorption at 340 nm after UV irradiation indicated the

dx.doi.org/10.1021/ac403920q | Anal. Chem. 2014, 86, 4783–4790

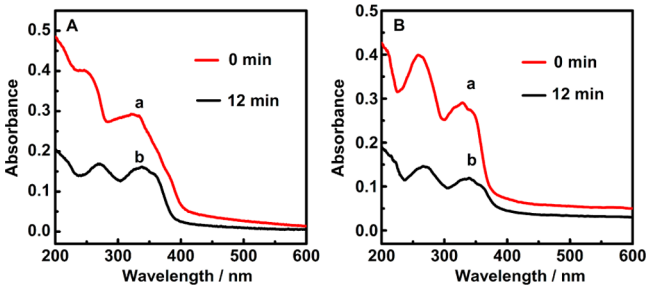

Figure 1. UV−vis spectra of the formylstyrylpyridine film (A) and $Mn_2P_2O_7$−formylstyrylpyridine film (B) on a quartz substrate without UV irradiation (a) and with (b) UV irradiation for 12 min. UV irradiation was performed with a high-pressure mercury lamp (365 nm).

consumption of SbQ groups.[16] In addition, a new shoulder peak appeared at around 270 nm, which was attributed to the nonconjugated aromatic ring of cyclobutane dimers.[16] The SbQ moiety was photoreactive and formed a dimer under UV irradiation. The associated reactive SbQ groups of formylstyrylpyridine formed covalent bonding via UV irradiation, which led to accelerate the rate of the formation the photopolymer film.[16] After adding $Mn_2P_2O_7$, the spectral change on the UV−vis absorption before (curve a) and after (curve b) UV irradiation was shown in Figure 1B. The change was the same as that of Formylstyrylpyridine film. The results demonstrated that $Mn_2P_2O_7$ was enwrapped by Formylstyrylpyridine polymer film under UV irradiation.

The TEM image of $Mn_2P_2O_7$ was displayed in Figure 2A. $Mn_2P_2O_7$ was multilayer sheet. Figure 2B showed the XRD

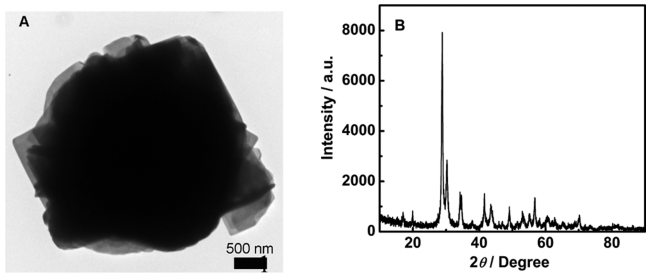

Figure 2. TEM image of $Mn_2P_2O_7$ (A), the accelerating voltage was 80 kV; XRD patterns of $Mn_2P_2O_7$ (B) in the range of $10 < 2\theta < 90°$.

pattern of $Mn_2P_2O_7$ prepared under the typical reaction conditions. The diffraction peaks in the range of $10 < 2\theta < 90°$ could be indexed as different planes of monoclinic phase $Mn_2P_2O_7$, which were in good accordance with the ASTM standard 72−2043.

Figure 3A and Figure 3B showed the SEM images of $Mn_2P_2O_7$−Formylstyrylpyridine without UV irradiation and with UV irradiation, respectively. Significant differences on the surface morphology could be observed. Without UV irradiation, $Mn_2P_2O_7$ could not be enwrapped well by the formylstyrylpyridine (Figure 3A). However, under UV irradiation, the aggregates of the trapped $Mn_2P_2O_7$ displayed a relatively uniform film (Figure 3B), which indicated the formation of specific interface.

Electrochemical Behavior of MWCNTs/$Mn_2P_2O_7$−Formylstyrylpyridine Modified Glassy Carbon Electrode (GCE). Figure 4 showed the CVs of different electrodes in 50 mmol L^{-1} K_3PO_4 solution at 100 mV s^{-1}. No electrochemical

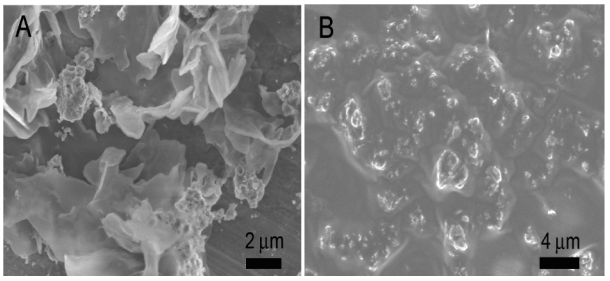

Figure 3. SEM images of $Mn_2P_2O_7$−formylstyrylpyridine without UV irradiation (A) and with UV irradiation for 12 min (B), respectively. The accelerating voltage was 10 kV.

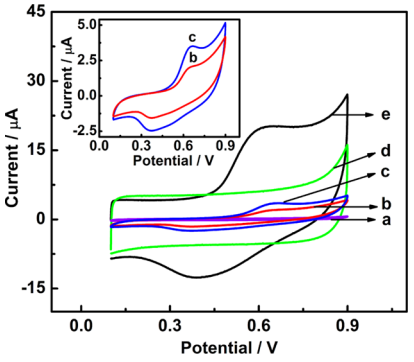

Figure 4. CVs of formylstyrylpyridine (a), $Mn_2P_2O_7$ (b), $Mn_2P_2O_7$−formylstyrylpyridine (c), MWCNTs/Formylstyrylpyridine (d), MWCNTs/$Mn_2P_2O_7$−formylstyrylpyridine (e) modified GCEs in 1.0 mL 50 mmol L^{-1} K_3PO_4 solution (pH 7.4). Inset: Magnified responses of $Mn_2P_2O_7$ (b) and $Mn_2P_2O_7$−formylstyrylpyridine (c) modified GCEs, respectively. Scan rate: 100 mV s^{-1}.

responses were obtained at both formylstyrylpyridine (curve a) and MWCNTs/formylstyrylpyridine modified GCEs (curve d). While one couple of well-defined redox peaks were observed at $Mn_2P_2O_7$ (curve b), $Mn_2P_2O_7$−formylstyrylpyridine (curve c) and MWCNTs/$Mn_2P_2O_7$−formylstyrylpyridine (curve e) modified GCEs. The anodic and cathodic peaks were attributed to the redox reaction of $Mn_2P_2O_7$. The response of $Mn_2P_2O_7$−formylstyrylpyridine modified GCE was much larger than that of $Mn_2P_2O_7$ modified GCE (insert in Figure 4). The experimental results demonstrated that formylstyrylpyridine could provide a biocompatible microenvironment for $Mn_2P_2O_7$ and subsequently provide a durable platform for determination of $O_2^{\bullet-}$. Moreover, MWCNTs/$Mn_2P_2O_7$−formylstyrylpyridine modified GCE showed the largest peak current (curve e). This might be due to excellent electronic conductivity of MWCNTs,[53,54] which would largely improve the sensitivity of bioanalysis. On the basis of these results above, the MWCNTs/$Mn_2P_2O_7$−formylstyrylpyridine films could be used to construct a biosensor for $O_2^{\bullet-}$ sensing and cell monitoring.

Electrochemical impedance spectroscopy was used to confirm the modification process of the biosensing interface based on MWCNTs/$Mn_2P_2O_7$−formylstyrylpyridine films. The Nyquist diagrams of electrochemical impedance spectra are shown in Figure S1 in Supporting Information. After the electrode was modified with MWCNTs (curve b), the semicircle domain became smaller comparing with that of the bare GCE (curve a). However, when $Mn_2P_2O_7$−formylstyrylpyridine added to the surface of MWCNTs modified GCE (curve c), the semicircle domain became larger comparing with that of the MWCNTs modified GCE (curve b). It may be due

dx.doi.org/10.1021/ac403920q | Anal. Chem. 2014, 86, 4783−4790

to the inferior conductivity of formylstyrylpyridine. From these results, the biosensing interface based on MWCNTs/$Mn_2P_2O_7$–formylstyrylpyridine films was verified to be constructed successfully through layer-by-layer assembly.

CVs obtained at MWCNTs/$Mn_2P_2O_7$–formylstyrylpyridine modified GCE with different potential scan rates were displayed in Figure S2 in Supporting Information. The reduction and oxidation peak currents of MWCNTs/$Mn_2P_2O_7$–formylstyrylpyridine modified GCE increased linearly with the scan rate in the range of 10–500 mV s^{-1}, while the difference of redox peak potentials showed slight increase, indicating a surface controlled electrode process.

Electrocatalysis of MWCNTs/$Mn_2P_2O_7$–Formylstyrylpyridine Modified GCE to the Oxidation and Reduction of $O_2^{\bullet-}$. As shown in Figure 5, with the addition of 100 μmol

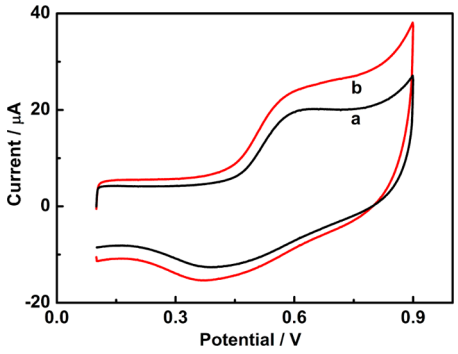

Figure 5. CVs of MWCNTs/$Mn_2P_2O_7$–formylstyrylpyridine modified GCE in the absence (a) and presence (b) of 100 μmol L^{-1} $O_2^{\bullet-}$ in 1.0 mL of 50 mmol L^{-1} K_3PO_4 solution (pH 7.4). Scan rate: 100 mV s^{-1}.

L^{-1} $O_2^{\bullet-}$ (curve b), anodic and cathodic peak currents, which were consistent with the redox reaction of $Mn_2P_2O_7$ in K_3PO_4 solution (curve a), both increased. This might be attributed to the oxidation and reduction of $O_2^{\bullet-}$, respectively. According to the previous report,[55] two $O_2^{\bullet-}$ were transformed into one O_2 molecule and one H_2O_2 molecule during the reaction of $O_2^{\bullet-}$ catalyzed by Mn^{2+} in K_3PO_4 solution, respectively. In the anodic process, the redox reaction between $O_2^{\bullet-}$ and MnO_2^+ took place to generate O_2 and Mn^{2+}. The generated Mn^{2+} could be reoxidized at the modified electrode. In the cathodic process, $O_2^{\bullet-}$ oxidized the Mn^{2+} to produce H_2O_2 and MnO_2^+. The generated MnO_2^+ could be reduced at the modified electrode. Namely, in the anodic process, $MnO_2^+ + 3O_2^{\bullet-} + 4H^+ = Mn^{2+} + 3O_2 + 2H_2O$; in the cathodic process, $Mn^{2+} + 3O_2^{\bullet-} + 2H_2O + 2H^+ = MnO_2^+ + 3H_2O_2$. Thus, $O_2^{\bullet-}$ could be detected by measuring the oxidation or reduction current at the MWCNTs/$Mn_2P_2O_7$–formylstyrylpyridine modified GCE in the presence of $O_2^{\bullet-}$ due to the high efficient catalysis of $Mn_2P_2O_7$.

Effects of Formylstyrylpyridine Concentration, Time of UV Irradiation, and Applied Potential on the Electrochemical Response. The electrochemical response depended on the amount of the formed complex film on the electrode surface. Formylstyrylpyridine largely affected electrochemical responses of the formed complex films due to its inferior conductivity of formylstyrylpyridine. Formylstyrylpyridine with different concentrations were mixed with $Mn_2P_2O_7$ and then added to the surface of MWCNTs modified GCE to form different MWCNTs/$Mn_2P_2O_7$–formylstyrylpyridine films modified GCEs. When the concentration of formylstyrylpyridine was 0.5 mmol L^{-1}, the reduction peak current reached a maximum value (Supporting Information Figure S3A). At this concentration of formylstyrylpyridine, MWCNTs/$Mn_2P_2O_7$–Formylstyrylpyridine films were performed by UV irradiation with different times (Supporting Information Figure S3B). The maximum reduction peak current occurred at 12 min under UV irradiation. Therefore, 0.5 mmol L^{-1} and 12 min were selected as the optimum concentration of Formylstyrylpyridine and time of UV irradiation, respectively. The applied potential was another important parameter for obtaining an optimal electrocatalytic response (Supporting Information Figure S3C). When the applied potential was 0.15 V, a largest response was achieved. Therefore, an applied potential of 0.15 V was chosen for the amperometric measurements.

Detection of $O_2^{\bullet-}$. At the applied potential of 0.15 V, the typical amperometric responses of MWCNTs/$Mn_2P_2O_7$–formylstyrylpyridine modified GCE to successive concentration changes of $O_2^{\bullet-}$ were examined and the corresponding current–time responses were displayed in Figure 6. The

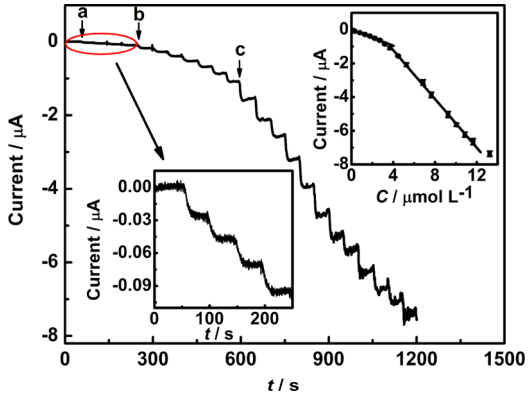

Figure 6. Successive amperometric responses of MWCNTs/$Mn_2P_2O_7$–formylstyrylpyridine modified GCE to KO_2 of different concentrations at applied potentials of 0.15 V in 1.0 mL 50 mmol L^{-1} K_3PO_4 solution (pH 7.4). From a to b, the KO_2 concentration of each adding step was 0.08 μmol L^{-1}; from b to c, each adding step was 0.4 μmol L^{-1} and after c each adding step was 0.8 μmol L^{-1}. Upper inset: Linear calibration curve of catalytic response of MWCNTs/$Mn_2P_2O_7$–formylstyrylpyridine modified GCE to KO_2 concentrations. Lower inset: Amplified response of the step marked with red circle.

response showed a linear increase with an increase in $O_2^{\bullet-}$ concentration from 0.08–3.19 and 3.67–11.65 μmol L^{-1} with correlation coefficient of 0.9915 and 0.9973, respectively. The linear range was wider than those of some other modified electrodes[33,56–59] (Table S1 in Supporting Information). The detection limit was estimated to be 0.029 μmol L^{-1} at a signal-to-noise ratio of 3:1, which was lower than those of some other modified electrodes and methods[60–64] (Table S2 in Supporting Information). The normal level of $O_2^{\bullet-}$ in physiological condition is about 0.1 μmmol L^{-1} and its concentration increases under traumatic brain injury ischemia-reperfusion, hypoxia, and other oxidative stress diseases.[65,66] Thus, the proposed amperometric biosensor showed promising application in the monitoring of $O_2^{\bullet-}$ with high sensitivity and wide concentration range due to the high efficient catalysis of $Mn_2P_2O_7$ and fast interfacial electron transfer at the surface of MWCNTs/$Mn_2P_2O_7$–formylstyrylpyridine modified films.

Selectivity, Stability, and Reproducibility of the $O_2^{\bullet-}$ Biosensor. To evaluate the selectivity of the proposed

dx.doi.org/10.1021/ac403920q | Anal. Chem. 2014, 86, 4783–4790

electrochemical biosensing system, a variety of relevant interfering species including DA, AA, Cys, O_2, H_2O_2, $OH^•$, $ONOO^-$, and Fe^{3+} in biological system was investigated for control experiments. 8.23%, 6.52%, 6.54%, 3.65%, 7.28%, 3.97%, 5.98%, and 14.27% of 1 μmol L^{-1} $O_2^{•-}$ cathodic current from 5 μmol L^{-1} DA, 10 μmol L^{-1} AA, 5 μmol L^{-1} Cys, 258 μmol L^{-1} O_2, 10 μmol L^{-1} H_2O_2, 10 μmol L^{-1} $OH^•$, 10 μmol L^{-1} $ONOO^-$, and 10 μmol L^{-1} Fe^{3+} were observed, respectively (Figure 7). No obvious interference was observed

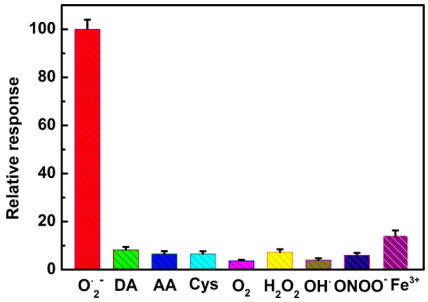

Figure 7. Effects of common interfering species including 5 μmol L^{-1} DA, 10 μmol L^{-1} AA, 5 μmol L^{-1} Cys, 258 μmol L^{-1} O_2, 10 μmol L^{-1} H_2O_2, 10 μmol L^{-1} $OH^•$, 10 μmol L^{-1} $ONOO^-$, and 10 μmol L^{-1} Fe^{3+} on the detection of 1 μmol L^{-1} $O_2^{•-}$ by using MWCNTs/$Mn_2P_2O_7$–formylstyrylpyridine modified GCE in 1 mL 50 mmol L^{-1} K_3PO_4 solution (pH 7.4) at an applied potential of 0.15 V.

upon $O_2^{•-}$ detection at 0.15 V. Therefore, the as-prepared electrochemical biosensor would have good selectivity for monitoring of $O_2^{•-}$ in biological samples. The stability of the fabricated biosensor was another important factor in practical applications. The long-term storage stability of the proposed biosensor was examined by measuring current response of the biosensor toward 5 μmol L^{-1} $O_2^{•-}$. After a storage time of 1 week in the shade at room temperature with measurements every few days, no obvious decrease of the current response to $O_2^{•-}$ was observed. After 4 weeks, the current response still retained 94.15% of its initial response, thereby suggesting that formylstyrylpyridine photopolymer film was very efficient for retaining the activity of immobilized SOD mimics and preventing them from leaking out of the biosensors. The fabrication reproducibility of five electrodes, made independently, showed an acceptable reproducibility with the relative standard deviation of 6.3% for the determinations of 5 μmol L^{-1} $O_2^{•-}$.

Cell Monitoring. As described above, the biosensor showed good analytical performance, which could be used in vitro determination of $O_2^{•-}$ released from living cells. 0.0002% glutaraldehyde was of lower toxicity to cells.[67,68] Further evidence came from MTT assay. The group without glutaraldehyde was considered as the control group and the cell viability was viewed as 100%. From the results shown in Figure S4 in Supporting Information, we can find that after cells were fixed with 0.0002% glutaraldhyde, the cell viability was almost preserved. The amperometric responses of the biosensor toward HeLa cells adhered on the biosensing interface in 1 mL K_3PO_4 solution (50 mmol L^{-1}) containing 50 mmol L^{-1} glucose were exhibited in Figure 8. After the addition of 4 μL 100 μg mL^{-1} PMA, which was reported to active NADPH oxidase (endogenous) and induce $O_2^{•-}$ generation from cells,[69−71] a much improved cathodic current was observed. Thus, the increased response was due to the

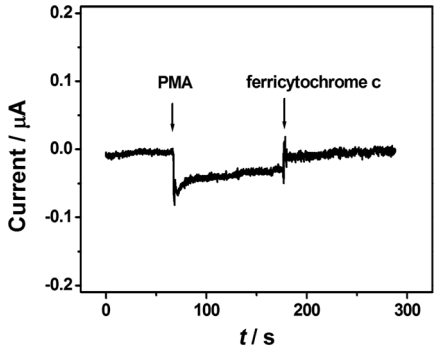

Figure 8. Amperometric responses of MWCNTs/$Mn_2P_2O_7$–Formylstyrylpyridine modified GCE to $O_2^{•-}$ released from Hela cells induced by PMA (400 ng mL^{-1}) and scavenged by adding 1 mmol L^{-1} ferricytochrome *c* in 1.0 mL 50 mmol L^{-1} K_3PO_4 containing 50 mmol L^{-1} glucose at an applied potential of 0.15 V.

biomimetic catalytic reduction of $O_2^{•-}$ released from living cells. A stable current of 33.5 nA was obtained at about 12 s after injection of PMA. This current corresponded to the $O_2^{•-}$ concentration of 87.9 nmol L^{-1}, which was calculated based on the calibration curve displayed in the upper inset of Figure 6. Because the pretreated cells (0.5 mL, 1×10^5 cells mL^{-1}) were plated on the modified electrode for electrochemical determination of $O_2^{•-}$, the amount of $O_2^{•-}$ was calculated to be 0.176 nmol per 10^5 cells, which was similar to 0.148 nmol per 10^5 cells releasing from embryonic striatal cells.[72] Thus, the mean flux of $O_2^{•-}$ releasing from the cells was evaluated to be 147 amol $cell^{-1}s^{-1}$. After the addition of PMA, 10 μL 100 mmol L^{-1} ferricytochrome *c* which acted as a selective scavenger of $O_2^{•-}$[73] was added, the current response of $O_2^{•-}$ decreased since the released $O_2^{•-}$ was scavenged by ferricytochrome *c*, further confirming that the enhancement of cathodic current was attributed to the electrochemical reduction of $O_2^{•-}$ catalyzed by $Mn_2P_2O_7$. Therefore, the biosensor could be used in living cells monitoring with ideal performance and studying the $O_2^{•-}$ generation in cells as well as quantifying the flux of $O_2^{•-}$ releasing from cells.

CONCLUSION

The novel MWCNTs/$Mn_2P_2O_7$–formylstyrylpyridine films under UV irradiation were prepared. MWCNTs enhanced the electrochemical responses because of their good conductivity. Formylstyrylpyridine was acted as a photopolymer material to immobilize $Mn_2P_2O_7$. Under UV irradiation, the aggregates of the trapped $Mn_2P_2O_7$ displayed a relatively uniform film and formed a specific interface. On the basis of fast interfacial electron transfer and the high efficient catalysis of $Mn_2P_2O_7$, which was used as a SOD mimic, a novel electrochemical biosensing platform for the $O_2^{•-}$ detection was developed. The proposed amperometric biosensor showed promising application in the determination of $O_2^{•-}$ with high sensitivity, wide concentration range, good selectivity, reproducibility, long-term stability and biocompatibility. The electrochemical biosensor provided a reliable platform to adhere living cells directly on the modified electrode surface. Using HeLa cells as a model, the biosensor was successfully applied to vitro determination of $O_2^{•-}$ released from living cells, which had a promising prospect for living cells monitoring and diagnosis of ROS-related diseases.

dx.doi.org/10.1021/ac403920q | *Anal. Chem.* 2014, 86, 4783−4790

■ ASSOCIATED CONTENT

Supporting Information

EIS of different modified electrodes, CVs of GCE/MWCNTs/$Mn_2P_2O_7$−formylstyrylpyridine at different scan rates, effects of formylstyrylpyridine concentration, time of UV irradiation, and the applied potential on the response of the biosensor, MTT results, and the linear range and detection limit of different modified electrodes for measurement of $O_2^{\bullet-}$. This material is available free of charge via the Internet at http://pubs.acs.org.

■ AUTHOR INFORMATION

Corresponding Author

*Fax: +86-25-85891051. Tel: +86-25-85891051. E-mail: daizhihuii@njnu.edu.cn.

Notes

The authors declare no competing financial interest.

■ ACKNOWLEDGMENTS

This research was supported by NSFC (21175069) and Foundation of the Jiangsu Education Committee (11KJA150003). We appreciate the financial support from the PAPD and the Program for Jiangsu Collaborative Innovation Center of Biomedical Functional Materials.

■ REFERENCES

(1) Sassolas, A.; Blum, L. J.; Leca-Bouvier, B. D. *Biotechnol. Adv.* **2012**, *30*, 489−511.
(2) Zhou, Z.; Hartmann, M. *Chem. Soc. Rev.* **2013**, *42*, 3894−3912.
(3) Cao, S.; Fang, L.; Zhao, Z.; Ge, Y.; Piletsky, S.; Turner, A. P. F. *Adv. Funct. Mater.* **2013**, *23*, 2162−2167.
(4) Shahdost-fard, F.; Salimi, A.; Sharifi, E.; Korani, A. *Biosens. Bioelectron.* **2013**, *48*, 100−107.
(5) Periyakaruppan, A.; Gandhiraman, R. P.; Meyyappan, M.; Koehne, J. E. *Anal. Chem.* **2013**, *85*, 3858−3863.
(6) Han, C.; Doepke, A.; Cho, W.; Likodimos, V.; de la Cruz, A. A.; Back, T.; Heineman, W. R.; Halsall, H. B.; Shanov, V. N.; Schulz, M. J.; Falaras, P.; Dionysiou, D. D. *Adv. Funct. Mater.* **2013**, *23*, 1807−1816.
(7) Papper, V.; Gorgy, K.; Elouarzaki, K.; Sukharaharja, A.; Cosnier, S.; Marks, R. S. *Chem.—Eur. J.* **2013**, *19*, 9639−9643.
(8) Lad, U.; Kale, G. M.; Bryaskova, R. *Anal. Chem.* **2013**, *85*, 6349−6355.
(9) Jang, H. D.; Kim, S. K.; Chang, H.; Roh, K. M.; Choi, J. W.; Huang, J. *Biosens. Bioelectron.* **2012**, *38*, 184−188.
(10) Vasylieva, N.; Maucler, C.; Meiller, A.; Viscogliosi, H.; Lieutaud, T.; Barbier, D.; Marinesco, S. *Anal. Chem.* **2013**, *85*, 2507−2515.
(11) Shtenberg, G.; Massad-Ivanir, N.; Moscovitz, O.; Engin, S.; Sharon, M.; Fruk, L.; Segal, E. *Anal. Chem.* **2013**, *85*, 1951−1956.
(12) Alves, N. J.; Mustafaoglu, N.; Bilgicer, B. *Biosens. Bioelectron.* **2013**, *49*, 387−393.
(13) Alves, N. J.; Champion, M. M.; Stefanick, J. F.; Handlogten, M. W.; Moustakas, D. T.; Shi, Y.; Shaw, B. F.; Navari, R. M.; Kiziltepe, T.; Bilgicer, B. *Biomaterials* **2013**, *34*, 5700−5710.
(14) Yang, X.; Tian, G.; Jiang, N.; Su, B. *Energy Environ. Sci.* **2012**, *5*, 5540.
(15) Ahuja, T.; Mir, I. A.; Kumar, D.; Rajesh. *Biomaterials* **2007**, *28*, 791−805.
(16) Sakamoto, T.; Nishimura, Y.; Nishimura, T.; Kato, T. *Angew. Chem., Int. Ed.* **2011**, *50*, 5856.
(17) Bayir, H. *Crit. Care Med.* **2005**, *33*, S498−501.
(18) Amatore, C.; Arbault, S.; Guille, M.; Lemaitre, F. *Chem. Rev.* **2008**, *108*, 2585−2621.
(19) Wang, W.; Fang, H.; Groom, L.; Cheng, A.; Zhang, W.; Liu, J.; Wang, X.; Li, K.; Han, P.; Zheng, M.; Yin, J.; Wang, W.; Mattson, M. P.; Kao, J. P.; Lakatta, E. G.; Sheu, S. S.; Ouyang, K.; Chen, J.; Dirksen, R. T.; Cheng, H. *Cell* **2008**, *134*, 279−290.
(20) Andersen, J. K. *Nat. Med.* **2004**, *10*, S18−25.
(21) Zweier, J. L.; Flaherty, J. T.; Weisfeldt, M. L. *Proc. Natl. Acad. Sci. U. S. A.* **1987**, *84*, 1404−1407.
(22) Vasquez-Vivar, J.; Hogg, N.; Pritchard, K. A., Jr; Martasek, P.; Kalyanaraman, B. *FEBS Lett.* **1997**, *403*, 127−130.
(23) Tsukagoshi, K.; Taniguchi, T.; Nakajima, R. *Anal. Chim. Acta* **2007**, *589*, 66−70.
(24) Diez, L.; Livertoux, M. H.; Stark, A. A.; Wellman-Rousseau, M.; Leroy, P. *J. Chromatogr. B* **2001**, *763*, 185−193.
(25) Fridovich, I. *J. Biol. Chem.* **1997**, *272*, 18515−18517.
(26) Ohyashiki, T.; Nunomura, M.; Katoh, T. *Biochim. Biophys. Acta* **1999**, *1421*, 131−139.
(27) Zhang, L.; Tang, B.; Ding, Y. *J. Agric. Food Chem.* **2005**, *53*, 549−553.
(28) Li, N.; Wang, H.; Xue, M.; Chang, C.; Chen, Z.; Zhuo, L.; Tang, B. *Chem. Commun.* **2012**, *48*, 2507−2509.
(29) Ohara, Y.; Peterson, T. E.; Harrison, D. G. *J. Clin. Invest.* **1993**, *91*, 2546−2551.
(30) Luo, Y.; Tian, Y.; Rui, Q. *Chem. Commun.* **2009**, 3014−3016.
(31) Wang, X.; Han, M.; Bao, J.; Tu, W.; Dai, Z. *Anal. Chim. Acta* **2012**, *717*, 61−66.
(32) Amatore, C.; Arbault, S.; Guille, M.; Lemaitre, F. *Chem. Rev.* **2008**, *108*, 2585−2621.
(33) Tian, Y.; Mao, L.; Okajima, T.; Ohsaka, T. *Anal. Chem.* **2002**, *74*, 2428−2434.
(34) Wang, L.; Wen, W.; Xiong, H.; Zhang, X.; Gu, H.; Wang, S. *Anal. Chim. Acta* **2013**, *758*, 66−71.
(35) Zhang, B.; Tang, D.; Goryacheva, I. Y.; Niessner, R.; Knopp, D. *Chem.—Eur. J.* **2013**, *19*, 2496−2503.
(36) Xu, Q.; Yan, F.; Lei, J.; Leng, C.; Ju, H. *Chem.—Eur. J.* **2012**, *18*, 4994−4998.
(37) Deng, Z.; Rui, Q.; Yin, X.; Liu, H.; Tian, Y. *Anal. Chem.* **2008**, *80*, 5839−5846.
(38) Rajesh, S.; Kanugula, A. K.; Bhargava, K.; Ilavazhagan, G.; Kotamraju, S.; Karunakaran, C. *Biosens. Bioelectron.* **2010**, *26*, 689−695.
(39) Dai, Z.; Liu, S.; Bao, J.; Ju, H. *Chem.—Eur. J.* **2009**, *15*, 4321−4326.
(40) Masini, E.; Bani, D.; Vannacci, A.; Pierpaoli, S.; Mannaioni, P. F.; Comhair, S. A.; Xu, W.; Muscoli, C.; Erzurum, S. C.; Salvemini, D. *Free Radical Biol. Med.* **2005**, *39*, 520−531.
(41) Shoji, E.; Freund, M. S. *J. Am. Chem. Soc.* **2001**, *123*, 3383−3384.
(42) Liu, R.; Li, S.; Yu, X.; Zhang, G.; Zhang, S.; Yao, J.; Keita, B.; Nadjo, L.; Zhi, L. *Small* **2012**, *8*, 1398−1406.
(43) Fu, B.; Cao, J.; Jiang, W.; Wang, L. *Biosens. Bioelectron.* **2013**, *44*, 52−56.
(44) Kramer, R. *Angew. Chem., Int. Ed.* **2000**, *39*, 4469−4470.
(45) Riley, D. P. *Chem. Rev.* **1999**, *99*, 2573−2588.
(46) Durot, S.; Policar, C.; Cisnetti, F.; Lambert, F.; Renault, J.-P.; Pelosi, G.; Blain, G.; Korri-Youssoufi, H.; Mahy, J.-P. *Eur. J. Inorg. Chem.* **2005**, 3513−3523.
(47) Clares, M. P.; Blasco, S.; Inclan, M.; del Castillo Agudo, L.; Verdejo, B.; Soriano, C.; Domenech, A.; Latorre, J.; Garcia-Espana, E. *Chem. Commun.* **2011**, *47*, 5988−5990.
(48) Wang, Q.; Zhang, B.; Lin, X.; Weng, W. *Sens. Actuators, B* **2011**, *156*, 599−605.
(49) Park, Y. T.; Park, J. Y.; Park, K.; Choi, S. S.; Yoo, Y. J. *J. Microbiol. Biotechnol.* **2008**, *18*, 1803−1808.
(50) Kawaguti, H. Y.; Buzzato, M. F.; Orsi, D. C.; Suzuki, G. T.; Sato, H. H. *Process Biochem.* **2006**, *41*, 2035−2040.
(51) Abe, K.; Saito, H. *Brain Res.* **1999**, *830*, 146−154.
(52) Hu, C.; Yang, D. P.; Wang, Z.; Yu, L.; Zhang, J.; Jia, N. *Anal. Chem.* **2013**, *85*, 5200−5206.
(53) Gao, C.; Guo, Z.; Liu, J. H.; Huang, X. J. *Nanoscale* **2012**, *4*, 1948−1963.
(54) Pumera, M. *Chem.—Eur. J.* **2009**, *15*, 4970−4978.
(55) Zhou, J.; Luo, Y.; Zhu, A.; Liu, Y.; Zhu, Z.; Tian, Y. *Analyst* **2011**, *136*, 1594−1598.

(56) Di, J.; Peng, S.; Shen, C.; Gao, Y.; Tu, Y. *Biosens. Bioelectron.* **2007**, *23*, 88−94.
(57) Wang, Y.; Wu, Y.; Wang, J. W.; Di, J. W. *Bioprocess. Biosyst. Eng.* **2009**, *32*, 531−536.
(58) Di, J. W.; Bi, S. P.; Zhang, M. *Biosens. Bioelectron.* **2004**, *19*, 1479−1486.
(59) Rafiee-Pour, H.-A.; Noorbakhsh, A.; Salimi, A.; Ghourchian, H. *Electroanalysis* **2010**, *22*, 1599−1606.
(60) Rajesh, S.; Kanugula, A. K.; Bhargava, K.; Ilavazhagan, G.; Kotamraju, S.; Karunakaran, C. *Biosens. Bioelectron.* **2010**, *26*, 689−695.
(61) Kim, S. K.; Kim, D.; You, J.-M.; Han, H. S.; Jeon, S. *Electrochim. Acta* **2012**, *81*, 31−36.
(62) Liu, H. Q.; Tian, Y.; Xia, P. P. *Langmuir* **2008**, *24*, 6359−6366.
(63) Kocabay, O.; Emregul, E.; Aras, S.; Emregul, K. C. *Bioprocess. Biosyst. Eng.* **2012**, *35*, 923−930.
(64) Yu, J.; Ge, L.; Liu, S.; Dai, P.; Ge, S.; Zheng, W. *Biosens. Bioelectron.* **2011**, *26*, 1936−1941.
(65) Hall, E. D.; Braughler, J. M. *Free Radical Biol. Med.* **1989**, *6*, 303−313.
(66) Floyd, R. A. *FASEB J.* **1990**, *4*, 2587−2597.
(67) Marczak, A.; Jozwiak, Z. *Toxicol. In Vitro* **2009**, *23*, 1188−1194.
(68) Marczak, A.; Bukowska, B. *Environ. Toxicol. Pharmacol.* **2013**, *36*, 171−181.
(69) Amatore, C.; Arbault, S.; Koh, A. C. *Anal. Chem.* **2010**, *82*, 1411−1419.
(70) Peshavariya, H. M.; Dusting, G. J.; Selemidis, S. *Free Radical Res.* **2007**, *41*, 699−712.
(71) Teufelhofer, O.; Weiss, R. M.; Parzefall, W.; Schulte-Hermann, R.; Micksche, M.; Berger, W.; Elbling, L. *Toxicol. Sci.* **2003**, *76*, 376−383.
(72) Ma, L.; Zhou, J. *Neurochem. Res.* **2006**, *31*, 463−471.
(73) Wegerich, F.; Giachetti, A.; Allegrozzi, M.; Lisdat, F.; Turano, P. *J. Biol. Inorg. Chem.* **2013**, *18*, 429−440.